

Geological and geochemical variations in Mid-Tertiary Ethiopian Flood Basalt Province, Maychew, Tigray Region, Ethiopia

Kurkura Kabeto*

Department of Earth Science, College of Natural and Computational Sciences, P.O. Box 231, Mekelle University, Ethiopia (*kurkura57@yahoo.com)

ABSTRACT

The paper presents the results of a comprehensive major element, trace element, and Sr-Nd-Pb-Hf isotopic study of Mid-Tertiary volcanic sequences from the northwestern flood basalt province in Ethiopia. The volcanic rocks studied range in composition from basanites, alkaline basalts, and ankaramites, which form the 1st three sequences at the base associated with basaltic agglomerate (sequence 1, 2 and 3) to transitional and tholeiitic basalts and picrites confined to the upper three sequences (sequences 4, 5 and 6). Sequence 5 is bimodal with intermediate-felsic pyroclastic rocks intercalating the transitional-tholeiitic basalts. There is a good correlation of sequences with geochemical enrichments, such as an increase La/Lu_N with TiO₂, and decrease in Al₂O₃ and SiO₂ towards the base. The smooth increase of La/Lu_N ratios in lower sequences reflect the general decrease of degree of partial melting that sampled heterogeneous packages of mantle plume materials. In the Sr-Nd isotopic diagram two clusters are formed one with restricted and low- Sr- (0.70356-0.70345) and Nd- (0.51290-0.51284) isotopic compositions, defined by sequence 1, and the other cluster with relatively higher ⁸⁷Sr/⁸⁶Sr (0.7052-0.7036) and ¹⁴³Nd/¹⁴⁴Nd (0.51296-0.5127) isotopic compositions defined by samples from sequence 2, and most other sequences with little scatter. The Pb-isotopic compositions vary systematically within each sequence (from base to top), and each sequence clustered systematically in a different Pb-Pb isotopic space with the highest ²⁰⁶Pb/²⁰⁴Pb (19.10-19.30) and ²⁰⁷Pb/²⁰⁴Pb (15.60-15.65) measured in sequence 1, quite differently from other sequences and from previously reported for northwestern Ethiopian flood basalt province, and the lowest ²⁰⁶Pb/²⁰⁴Pb (18.20-18.56) and ²⁰⁷Pb/²⁰⁴Pb (15.51-15.55) measured in sequence 4. Sequence 2 and 3 lavas display a similar ²⁰⁶Pb/²⁰⁴Pb and ²⁰⁷Pb/²⁰⁴Pb ranges falling between sequence 1 and 4. In contrast, sequence 6 samples displayed towards higher ²⁰⁶Pb/²⁰⁴Pb than sequence 2, 3, and 4, but with lower and higher ²⁰⁷Pb/²⁰⁴Pb than sequence 1 and 5 respectively. The lavas of sequence 1 and 4 have relatively less radiogenic ¹⁷⁶Hf/¹⁷⁷Hf than other sequences with slight scatter. The systematic geochemical variations in lavas are remarkable and reflects three mantle end component mixing with minimal crustal input as a fourth component. The enriched sequence 1 has very similar geochemistry to HIMU-type ocean island basalts (OIBs), and this end member ascribed to be the most enriched Afar plume component 1, which is the most enriched Afar Plume component during initial continental break. The second enriched component is defined by sequence 2 and 3 samples and may reflect the second enriched component in Ethiopian flood basalt, previously reported for the high-Ti2 basalts assumed to be the enriched Afar Plume component, whereas the third component is the depleted component defined by sequence 4 partly overlap the range previously reported for low-Ti basalts.

Keywords: Flood basalts, Geochemistry, Sr-Nd, Pb-Pb, Hf-Hf isotopes, Afar Plume, Partial melting, Crustal input.

1. INTRODUCTION

The Mid-Tertiary (~30 Ma) Ethiopian continental flood basalts form part of the larger Afro-Arabian Igneous Province, which is related to the Afar plume and the Red Sea-Gulf of Aden - Ethiopian Rift triple junction. Maychew, the area, of present study (Fig. 1) forms part of the high-Ti basalts of Ethiopian flood basalt province. Rocks here are composed of alkaline lavas (basanites, basalts, and ankaramites, with basaltic agglomerate) at the base, felsic volcanics in the middle, and transitional to tholeiitic mafic lavas at the top of the transitional sequence. Pik et al. (1998, 1999) have classified the north-western Ethiopian flood basalts into three distinct geochemical groups based on trace element and Ti concentrations: low-Ti basalts (LT), high-Ti1 (HT1) basalts and high-Ti2 (HT2) basalts. They recognized a suite of 'low-Ti' (LT) basalts restricted to the northwestern part of the province (Fig. 1) assumed to be derived from depleted mantle. They are characterized by relatively flat REE patterns and lower Ti and incompatible trace element concentrations. Alkali basalts found to the south and east of the province on the other hand show higher concentrations of incompatible elements and more fractionated REE patterns and related to the so-called 'high-Ti' basalts (HT1 and HT2).

In Western Ethiopian Plateau, up to 2 km thick predominantly mafic lavas with minor felsic pyroclastics (Fig. 1) make up the northern part of the Ethiopian flood basalt sequence (e.g., Hoffman, 1997; Ayalew et al., 2002) and cover an area of ~ 106 km³ (Rochette et al., 1998). The Maychew area is located in the northern eastern corner of the western Ethiopian plateau and covers an area of about 100 km². At present there is no geochronological data available for Maychew lavas to verify the sequential variations, but the earlier K-Ar whole-rock age dating of basalts collected from 110 m and 140 m above base in Maychew area gave 26.2 Ma and 25.7 Ma (Jones, 1976), respectively. However, such a young age compared to the current refined and accepted mineral ⁴⁰Ar/³⁹Ar age of 30.9 and 29.2 Ma for the northwestern Ethiopian continental flood lavas (Hofmann et al., 1997; Coulie et al., 2003; Kieffer et al., 2004) could be related to the unrecognized argon loss or gain in these intensely weathered formations. Hence, at present 31-29 Ma is accepted as a reasonable estimate for the Maychew flood basalt sequence. As shown in figure 1, the Maychew area is located between the Adigrat area and Chinese road section (A and C, in Fig. 1) and the samples collected from these areas are dated between 31-29 Ma. Moreover, recently Kieffer et al. (2004), dated plagioclase separate from alkaline picrite from Bora

Mountain (B in Fig. 1, close to Maychew area) at 30.99 ± 0.13 Ma. The dated sample is taken from lateral variation of ankaramite/ picrite of sequence 2 (Fig. 2). The younger age of 29.2 Ma (Hofmann et al., 1997) is obtained from ignimbrite layers exposed at the top part of the sequences, which is equivalent to sequence 5 described at Maychew area.

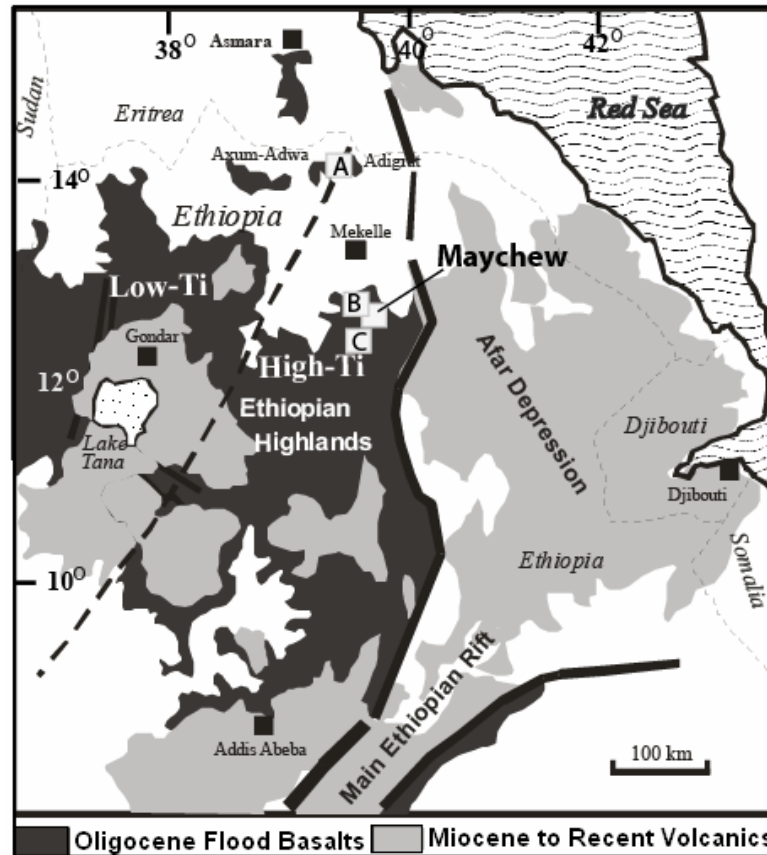


Figure 1. Location map of NW Ethiopian Plateau, Afar Rift and Main Ethiopian Rift (from Kuster et al., 2005). The approximate broken line separates the low-Ti and High-Ti flood basalt province (Pik et al., 1998).

Despite a relatively large chemical database for the southern and western Ethiopian plateau volcanics, there are still many parts of the plateau magmatism that are not studied. Most studies on Ethiopian rift and plateau magmatism have been carried out at a regional scale (Pik et al., 1999, Kieffer et al., 2004), and detailed investigations on single sections of the plateau are scarce. Moreover, lack of a detailed geological map of any particular section of the Ethiopian flood basalt province makes it difficult to correlate much of the existing high quality geochemical data from various parts of the Ethiopian flood basalt province. This paper presents

geology map of part Maychew area dominated by high-Ti basalts (Figs.1; 2 & 3). Systematic rock sampling of selected sections was carried out. They are analysed for whole-rock major and trace elements, Sr, Nd, Pb, and Hf isotopic data using suitable procedures (Nakamura et al., 2003) at Pheasant Memorial Laboratory of the Institute for study the earth's Interior, Okayama University at Misasa. The large data set of the volcanics thus obtained is discussed in the paper in addition to geology and stratigraphic sequence of the flows.

2. STRATIGRAPHIC SEQUENCES, PETROGRAPHIC DESCRIPTION OF VOLCANICS OF MAYCHEW AREA

Geology of Maychew area covered in this paper includes many lithological units (Figs. 2 & 3) and the volcanic successions which reveal six cycles (referred as sequence, Kabeto et al., 2004). Out of six, four are related to mafic-agglomerate volcanism (exposed between 1800-2900 m a.s.l, sequences 1, 2, 3, and 4), in which basanites, and alkaline basalts and transitional ankaramites occupy the base (sequences 1, 2 and 3) followed by silica rich tholeiitic to transitional sequence 4. This is followed by sequence 5 of mafic-felsic volcanism (2900-3450 m) and that is covered by tholeiitic to transitional basalts of sequence 6 (3450-3780 m); and represent the last stage of flood basalt volcanism in the Eastern part of northwestern Ethiopian plateau flood basalts. The lower most mafic sequence (Sequence 1) is in fault contact with Cretaceous Amba Aradam Sandstone, indicating that the base of the sequence is not exposed (Figs. 2 & 3). The sequences lack major unconformities; although intercalations of 10-20 cm thick paleosols are common in some sequences otherwise volcanism and depositions were continuous (Fig. 3). The lower three sequences (1, 2 & 3) are more disturbed and tilted at 4-25° towards SE than upper 3 sequences (4, 5 & 6). However, along NNE-SSW, NNW-SSE, and ENE-WSW striking normal faults they are also weakly tilted at about 3-4°, and disturbed. The altitude sub-division used above may vary depending on these normal faults throw, which is clear at Bekura and Tsibet mountains (Figs. 2 & 3). There is evidence of deformation of the type that Merla (1979) and Brehe et al. (1987) used to differentiate the deformed lower and upper undeformed formations, however, such evidence was not observed in the northwestern part of the plateau (Kieffer et al., 2004).

In Maychew area, there is a marked change in the morphology. Sequence 1, 2, and 3 are marked by deformed and subdued topography. However, sequence 2 also display gently undulating

morphology and the steepness of the slope is passing from sequence 2 to 3 and the first sharp cliff marks sequence 4. The exposure of sequence 5 is marked by broken flat surface where the andesitic pyroclastics nearly eroded to flat surface (suitable agricultural land) and a resistant pediment made up of picrite and ankaramite. 2 sharp cliffs one in the middle and the other on top is marked by 15 to 10 m thick consolidated tuff and ignimbrite partly showing columnar joints. The last sequence forms tabular facies, in which flow units are about 12 m thick, alternate with braided lobes of pahoehoe of ~1 to 3 m thick. The sequence 2 and 3 resemble the high-Ti₂ and the other sequences (4, 5, and 6) might be considered as high-TiO₂ 1 of Pik et al. (1998, 1999). However, sequence 1 is described for the first time in the Ethiopian Plateau Geology (Kabeto et al., 2004, 2006). There is systematic variation in the characteristics of the dominant volcanic rocks from the base (1800 m, Mehoni plain) of the Maychew volcanic sequence to the summit at the Tsibet Mountain (3780 m) (Figs. 2 & 3) and these sequences are described below.

2.1. Sequence 1: Deeply weathered and often tilted basanite and basaltic agglomerate intercalations (~between 1800 and 2500 m). Sequence 1 ranges in maximum thickness from 100-150 m and mark the base of exposed flood basalt province (at Mehoni plain and at the base of Bekura Mt.), and comprise many individual flows. Typically occur as a series of stacked flows 2-6 m thick separated at places by paleosol horizons (5-20 cm). Basanitic agglomerate layers are also common. The massive flows contain very few microphenocrysts (< 2%) of greenish elongated clinopyroxene (diopsidic) and Fe-Ti oxides with rare olivine mostly altered, in the groundmass of clinopyroxene, phlogophite, opaque, glass and rare plagioclase.

2.2. Sequence 2: It ranges in thickness from 450-600 m (~ 2000-2500 m) and comprise many individual flows. It is strongly weathered and tilted. The alkaline basalt and ankaramite flows typically occur as a series of stacked flows 1-10 m thick separated commonly by patchy basaltic agglomerate (1-10 m) layers. The mafic lava flows of this sequence consist of four litho-types, ankaramite, aphanitic basalts, porphyritic basalts and basaltic agglomerates. Porphyritic basalts and ankaramite predominates and often contain phenocryst (10-80%) of greenish and brownish clinopyroxene (zoned) and olivine, which are commonly iddingsitised. Fe-Ti oxides, plagioclase, clinopyroxene and glass form the microphenocryst and groundmass phases. Few ankaramites contain abundant olivine phenocryst compared to clinopyroxene. The aphanitic flows are generally microcrystalline with few pyroxenes and altered olivine microphenocrysts and often

form the base and top of the sequence.

2.3. Sequence 3: It consists of ankaramite, phyric basalts and agglomerate intercalations (~2500-2700 m) and ranges in thickness from 150-200 m. It comprises many individual massive cumulative ankaramites and porphyritic basalts (Fig. 3). The lavas typically occur as a series of massive to blocky bodies of 30-40 m thick separated by patchy agglomerate (~2 m) and phyric basalt (2-3 m) layers. The ankaramites range in composition from pyroxene-rich at base to plagioclase-rich in the top and olivine gabbros at the middle that form intergranular/gabbroic texture consisting of dominantly Ti-augite (3-6 mm), followed by plagioclase (2-3 mm), olivine and Fe-Ti oxides (1-2 mm), forming seriate texture. The top part of sequence 3 is plagioclase dominant basalt.

2.4. Sequence 4: Cliff forming aphyric to phyric basalts and basaltic agglomerate intercalations (~2700-2900 m), and has a maximum thickness of 200 m (Fig. 2). The transitional to tholeiitic basaltic flows typically comprise many horizontally stratified flows of 1-5 m thick separated by patchy basaltic agglomerate (0.5-1 m). The lava flows consist of three litho-types, aphanitic, and slightly porphyritic basalts, and basaltic agglomerate. Flows in this sequence typically contain up to 10% plagioclase phenocryst in a pilotaxitic groundmass of predominantly plagioclase microlites, pyroxene, and Fe-Ti oxides and glass now altered partly to chlorite and epidote. Trachytic texture is common, and few samples contain microphenocryst of brownish clinopyroxene, Fe-Ti oxides, and olivine.

2.5. Sequence 5: The sequence marks the bimodal volcanic activity in the northwestern Ethiopian flood basalt province (~2900-3450 m). The pyroclastic rocks consist of two litho-types: greenish to yellowish-grey andesitic tephra and grey trachy-rhyolitic ignimbrite. Greenish to grey varieties form the basal part of the pyroclastic flow deposits, whereas welded variety form the top part even grading to thinly banded rhyolite (20-35 cm) flows at the top of the ignimbrite layers (Fig. 2). In between the basal andesitic tephra and the top ignimbrite and rhyolite flows, phyric to aphyric basalts and picrite-ankaramite occur (Fig. 2). Greenish andesitic tephra variety predominates and they form crystal, rock, and glass fragments in glassy rarely devitrified and epidotized groundmass. The crystals are commonly plagioclase, aegirine-augite, and opaques possibly Fe-Ti oxides. In the ignimbrites, aegirine-augite and abundant sanidine with few opaque and anorthoclase, and rare rock fragments together form the fragmental part.

Variably weathered and partly welded glassy ash forms the groundmass. Olivine rich ankaramite show intergranular texture consists of dominantly olivine, clinopyroxene, and plagioclase. Samples taken from Aygi section is commonly olivine picrites, where olivine predominates over clinopyroxene and plagioclase, whereas from Tsibet mountain section (Figs. 2 & 3), clinopyroxene and plagioclase predominate over olivine and at places range to olivine gabbro composition similar to sequence 3 ankaramites.

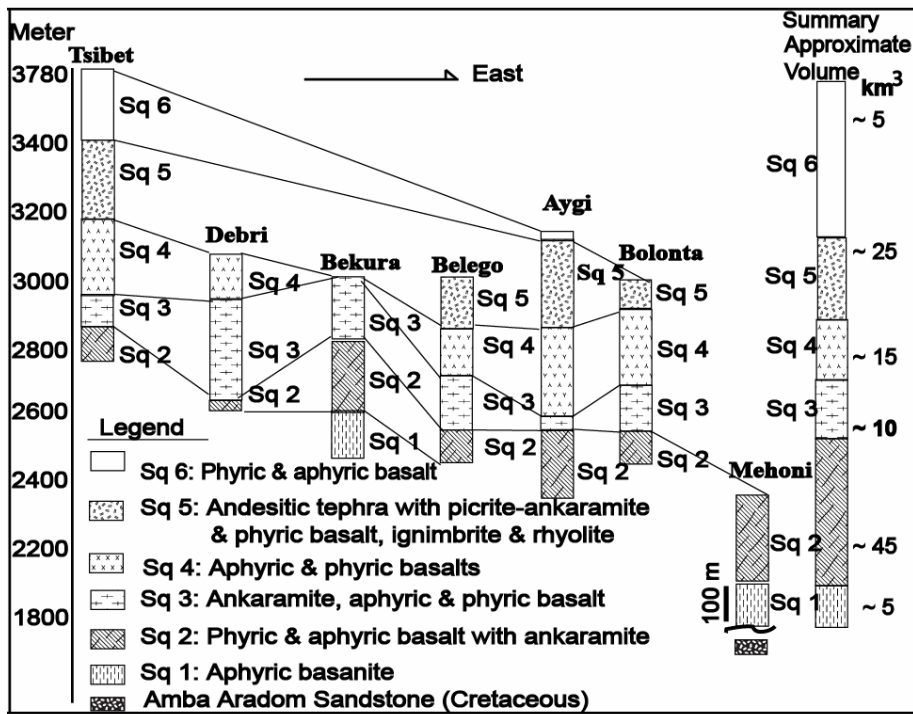


Figure 2. Schematic columnar section of Maychew area (modified from Kabeto et al., 2004). Numbers on the left side are elevations in meter above sea level. Abbreviation: Sq1 = Sequence 1. The scale on the right of lithological column is in hundreds of meters.

2.6. Sequence 6: The upper part of the flood basalt sequences in Maychew area is marked by unimodal, 330 m thick transitional to tholeiitic basalt of sequence 6 (3450-3780 m), and comprise many series of horizontally stratified massive to blocky jointed 5-10 m thick lava sequence. Porphyritic basalts which predominate the sequence consist of plagioclase (up to 20%) forming commonly glomeroporphyritic clots with rare clinopyroxene, olivine, and microphenocrysts of Fe-Ti oxides in the pilotaxitic groundmass of plagioclase, opaque, clinopyroxene, and glass. The groundmass in some thin sections is altered to chlorite. In rare

case olivine (3-5 mm) also form the dominant phenocryst phase.

The petrographic study of Maychew mafic lavas show systematic phenocryst assemblage variations starting from base to top, where at the base very few microphenocrysts of clinopyroxene characterizes sequence 1 (basanite). The predominance of clinopyroxene phenocryst with appearance of olivine in most samples typifies sequence 2. Sequence 3 is characterized by appearance of plagioclase and predominance of clinopyroxene and olivine (ankaramite), whereas plagioclase predominate the phenocryst phase in sequence 4. Olivine predominates the phenocryst phase over plagioclase and pyroxene in sequence 5; and plagioclase

in sequence 6 with some variations.

Further, the geological traverses taken in seven different sections (Fig. 2) indicate the missing of sequences from some sections. For example sequence 1 is absent in Debri, Tsibet, and Belego sections, whereas sequence 5 is only exposed in Tsibet, Belego, Aygi, and Bolonta sections. Moreover, Bekura section lacks sequences 4, 5, and 6, and sequence 6 exposed on top of Aygi and Tsibet section (Figs. 2 & 3). Missing of the sequences in the area seems to be due to normal faulting and erosion. This suggests the need for detailed mapping in previously studied sections of the Ethiopian plateau.

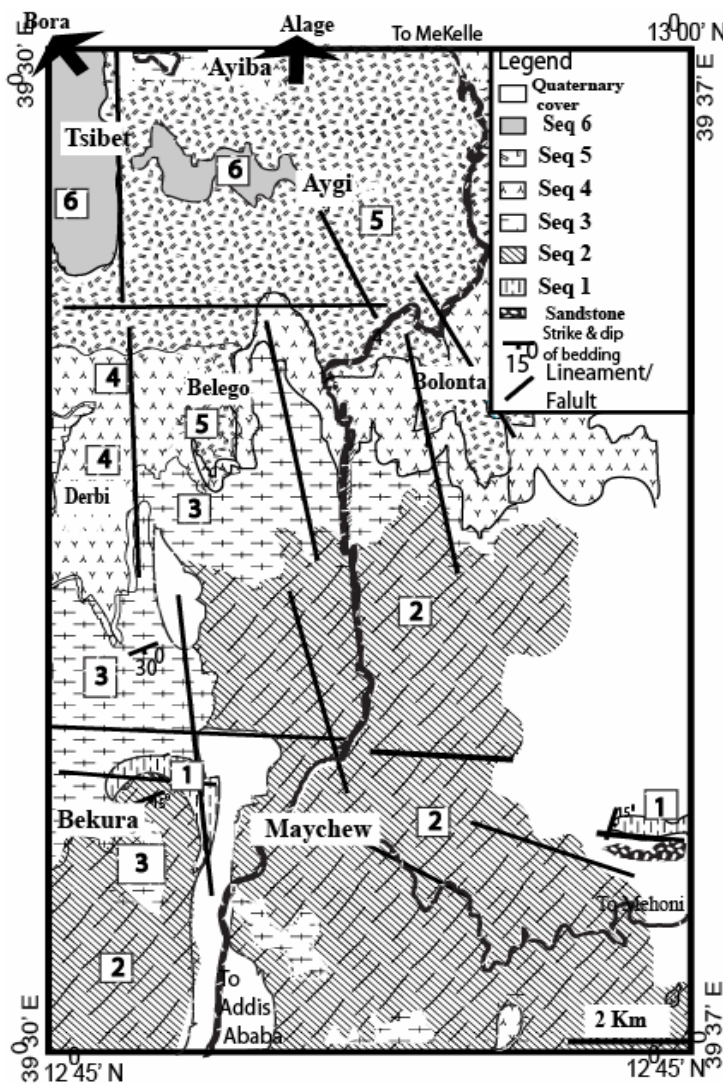


Figure 3. Geological map of Maychew area (Numbers on the map indicate sequences as shown in Figure 2. Bora is 20 Km NW and Alage is 20 Km north of the map area).

3. SAMPLING STRATEGY AND ANALYTICAL METHODS

Geological mapping activity and samples of all possible fresh volcanic rocks exposed within the study area were collected during three separate field seasons. Seven different transects were selected within 100 km², to enable detail mapping, and sampling a wide, a diversity of temporal and spatial chemical variations as possible in a high-Ti zone of the flood basalt sequence.

The samples were analyzed for whole-rock major and trace elements, and Sr-, Nd-, Pb-, and Hf-isotopic data at the Pheasant Memorial Laboratory (PML), Institute for study the earth's Interior, Okayama University at Misasa. A total of 89 whole-rock samples were crushed using jaw crusher to coarse chips of 3-5 mm size, from which fresh chips were carefully hand-picked. They were rinsed with deionized water in an ultrasonic bath at least three times, and then they were dried at 100°C for 12 hours. The washed and dried chips were ground using an alumina puck mill. Major elements, Ni and Cr data were obtained using X-ray fluorescence spectrometer (XRF) (Phillips PW2400) on glass beads containing a lithium tetraborate flux (10 to 1 dilution of samples) (Takei, 2002). Loss on ignition (LOI) was obtained gravimetrically. Trace elements were determined by isotope dilution (ID) and analyzed by inductively coupled plasma mass spectrometry (ICP-MS) using a Agilent 7500cs system fitted with a flow injection system (Makishima & Nakamura, 1997; Makishima et al., 1997, 1999; Yokoyama et al., 1999; Moriguti et al., 2004). Isotopes data for Rb, Sr, Sm and Nd were generated for the samples selected for Sr-Nd isotopic measurement, by isotope dilution thermal ionization mass spectrometry using a modified Finnigan MAT261 instrument with NBS983 standard. Trace element concentrations in CaO- rich samples were measured by the Al-addition methods as suggested by Tanaka et al. (2007 & reference therein). All of the major and trace elements analyses were duplicated for each sample, and replicate analyses had <0.5 relative % and 3-5 relative % difference, for major and trace elements, respectively.

The analytical procedures for chemical separation and mass spectrometry followed in the study are from Yoshikawa & Nakamura (1993) for Sr isotope measurements; Makishima & Nakamura (1991) for Nd; Kuritani & Nakamura (2002) for Pb; and Lu et al. (2007) for Hf. To remove the effect of secondary alterations (after petrographic examinations) all powders for Pb- and Hf- and some samples for Sr-Nd- isotopic measurements were leached with 6N HCl at 70°C for about 9 hours, before acid digestions.

Mass spectrometry was carried out with TIMS system in static multi-collection mode. Normalizing factors to correct isotopic fractionation during spectrometer analysis are $^{86}\text{Sr}/^{88}\text{Sr} = 0.1194$ for Sr and $^{146}\text{Nd}/^{144}\text{Nd} = 0.7219$ for Nd. The isotopic composition of NIST SRM987 and LaJolla standards are $^{87}\text{Sr}/^{86}\text{Sr} = 0.710190$ and $^{143}\text{Nd}/^{144}\text{Nd} = 0.511863$, respectively (Makishima & Masuda, 1993) and are reported relative to long-term (over 2 years) laboratory averages. For Pb isotope measurements the correction of mass fractionation was carried out by the normal double spike method using a ^{207}Pb - ^{204}Pb spike, as described by Kuritani & Nakamura (2003). The isotopic composition of NIST SRM981 Pb standard gave an average ($n = 5$) of $^{206}\text{Pb}/^{204}\text{Pb} = 16.9424 \pm 11$ (2σ), $^{207}\text{Pb}/^{204}\text{Pb} = 15.5003 \pm 12$ (2σ), and $^{208}\text{Pb}/^{204}\text{Pb} = 36.7266 \pm 60$ (2σ) (Kuritani & Nakamura, 2003). $^{176}\text{Hf}/^{177}\text{Hf}$ of the JMC475 and JMC14374 Hf standards yield averages of 0.282150 ± 6 (2σ , $n=9$) and 0.282187 ± 8 (2σ , $n=13$), respectively during the course of analysis. All Hf (Makishima et al., 1999) isotope data for the samples are, however, reported relative to $^{176}\text{Hf}/^{177}\text{Hf}$ of the JMC475 = 0.282160.

4. RESULTS AND DISCUSSION

4.1. Classification of the volcanic flows/sequences

According to the total alkali-SiO₂ classification diagram (Fig. 4), mafic rock types range in composition from basanite, picrite-ankaramite, basalt to basalt-trachy-andesite. But transitional to sub-alkaline basalts predominate. In contrast with many continental flood basalts, the mafic rocks at Maychew area do not entirely show tholeiitic affinities and also do not fall in the basalt field (Fig. 4). Based on the petrographic data and lithological assemblages the different mafic lavas are subdivided in to six sequences from base to top. General characteristics of the mafic rocks are illustrated in the total alkalis–silica (TAS) diagram (Fig. 4).

The Maychew sequences have compositions that plot, with some exceptions, in the alkaline and sub-alkaline field, respectively. According to the proposed classification of Ethiopian flood basalts (Piccerillo et al., 1979), the sequences 1 and 2 are alkaline in composition, whereas sequences 3 and 4 lavas have compositions that plot between alkaline (few) and sub-alkaline field, indicating transitional character. However, the sequence 4 shows higher SiO₂ contents and/or higher Na₂O + K₂O (up to 5.2 wt.%) contents and some samples plot in the alkali field when compared to sequence 5 and 6 samples, which have lower SiO₂ and Na₂O + K₂O (< 3.5

wt.%) and plotted towards tholeiitic field line. These distinctions extend to other incompatible major and trace elements. In this study three samples from sequence 2, twelve samples from sequence 3, and five samples from sequence 5 are plotted in picrite field, having MgO contents > 12 wt.% and total alkalis < 3 wt.% (Fig. 4), as per IUGS classification (Le Bas, 2000). However, as per petrographic data these samples (picrite) since dominant in clinopyroxene, are assigned as ankaramitic picrites, whereas samples with olivine dominant as picrites.

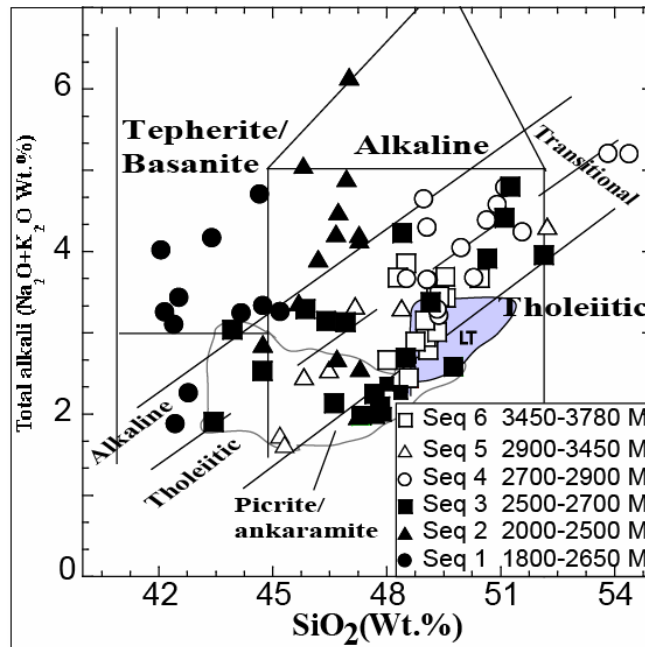


Figure 4. Total alkali Silica Classification of Maychew lavas compared with the low-Ti (LT) basalts (Pik et al., 1998).

The low-Ti basalts (LT shaded, Fig.4) (Pik et al., 1998; Kieffer et al., 2004) are compared with Maychew lavas.

4.2. Major element compositions of mafic rocks from the Maychew flood basalt section

General characteristics of the mafic rocks are illustrated in the total alkalis–silica (TAS) diagram (Fig. 4), and plots of the selected major and trace elements versus MgO shown in figure 5. The lavas from sequence 1 and 2 are referred as basanites because with two or three exceptions majority samples plot in the alkaline field. On the other hand, the lavas from sequences 3 and 4 are referred to as transitional ankaramite and basalt respectively as they plot in the transitional

field and from sequences 5 and 6 are referred to as tholeiitic picrites-ankaramite and basalts as they plot though within the transitional field but towards tholeiitic affinity. The Maychew lava sequences can be broadly grouped from base to top as strongly alkaline, transitional, and tholeiitic and these subdivisions also well reflected in major oxides, trace element, and Sr-, Nd-, Pb-, and Hf- isotopic compositional variations. The mafic lavas span a large range in MgO, from primitive (~23 Wt. %) to evolved (~4 Wt. %) compositions. In general, the ankaramites and picrites from sequences 3 and 5 show highest MgO content and the transitional basalts of sequence 4 the lowest. Sequence 3 displays a wide variation in MgO content followed by sequences 5 and 2. SiO₂ content (Figs. 4 & 5) for the Maychew mafic lavas ranges from 42 to 54 Wt. %, basanites < 45 Wt.% (Seq.1) and transitional basalts > 48 Wt.% (Seq.4). SiO₂, Al₂O₃, TiO₂, and K₂O (not shown) contents display broad negative correlations with MgO, whereas CaO content in sequences 2, 3 and 5 shows initial negative correlation with MgO till the content reached 12 Wt.%, afterwards the correlation becomes positive. Sequences 1, 4 and 6 (if MgO rich sample is excluded) on the other hand display positive correlation compared to others indicating their differentiated nature. Basanite (Seq.1) shows significant compositional difference than other sequences i.e. lowest in SiO₂ and Al₂O₃, highest in FeO_{total}, CaO and MnO (not shown) contents. Further, alkaline basalt of sequence 2, also shows lower values for SiO₂ and Al₂O₃ than the sequences upwards, but display higher FeO_{total} and TiO₂ contents. On the contrary, sequences 5 and 6 show lower values for TiO₂ and the highest for Al₂O₃ with few exceptions that overlap sequences 4 and 3. K₂O content is variable in most sequences, it is relatively higher in sequence 3 than sequence 4 at a given MgO content except with few overlap. Similar difference can be inferred from contents of CaO and TiO₂. Major element chemical variations within each sequence can be largely explained by crystal fractionation involving olivine, clinopyroxene, iron-titanium oxides, and plagioclase, however, difference in TiO₂, CaO, K₂O, Al₂O₃ and to some extent in SiO₂ and FeO_{total} among the six sequences reflect source variations or/and variable degrees of partial melting.

In figure 5, major element vs. MgO, majority elements clearly show existence of compositional variations among sequences. However, in some cases there is an overlap e.g. sequence 3 and 2 overlap in more mafic compositions, but their evolved varieties differ in TiO₂, FeO_{total}, Al₂O₃, and SiO₂ content. Similarly, the sequences 3 and 4 indicate overlap in their evolved varieties in

MgO vs. Al_2O_3 , SiO_2 , FeO_{total} and TiO_2 , but they do differ in K_2O and CaO contents (Fig. 5d).

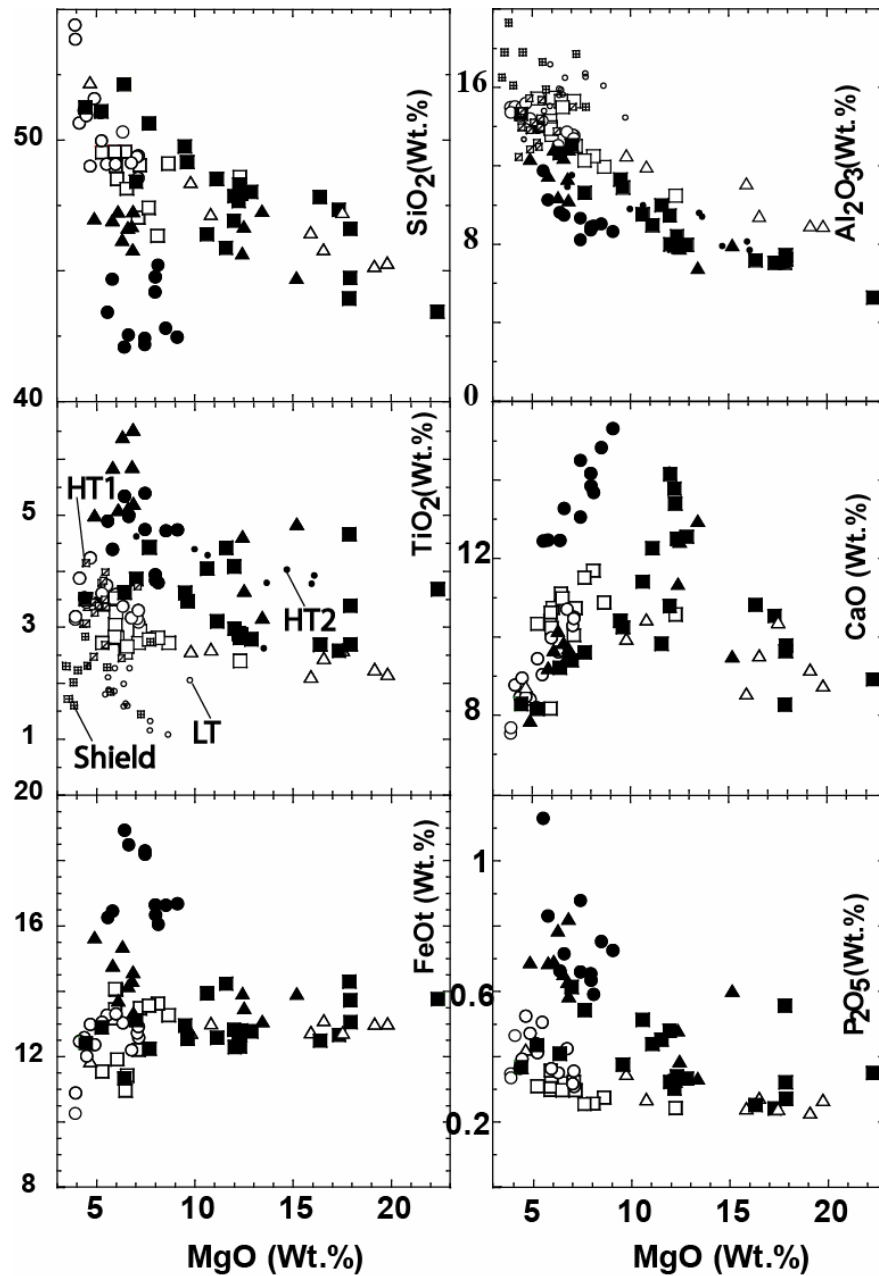


Figure 5. MgO vs. selected major oxides for Maychew lavas. LT, HT1, and HT2 and Shield basalts are taken from Pik et al. (1998); and Kieffer et al. (2004).

The notable compositional variation in SiO_2 , Al_2O_3 , TiO_2 , P_2O_5 , FeO_{total} , and CaO among the lavas will further demonstrate the existence of rather six sequences (1, 2, 3, 4, 5, and 6).

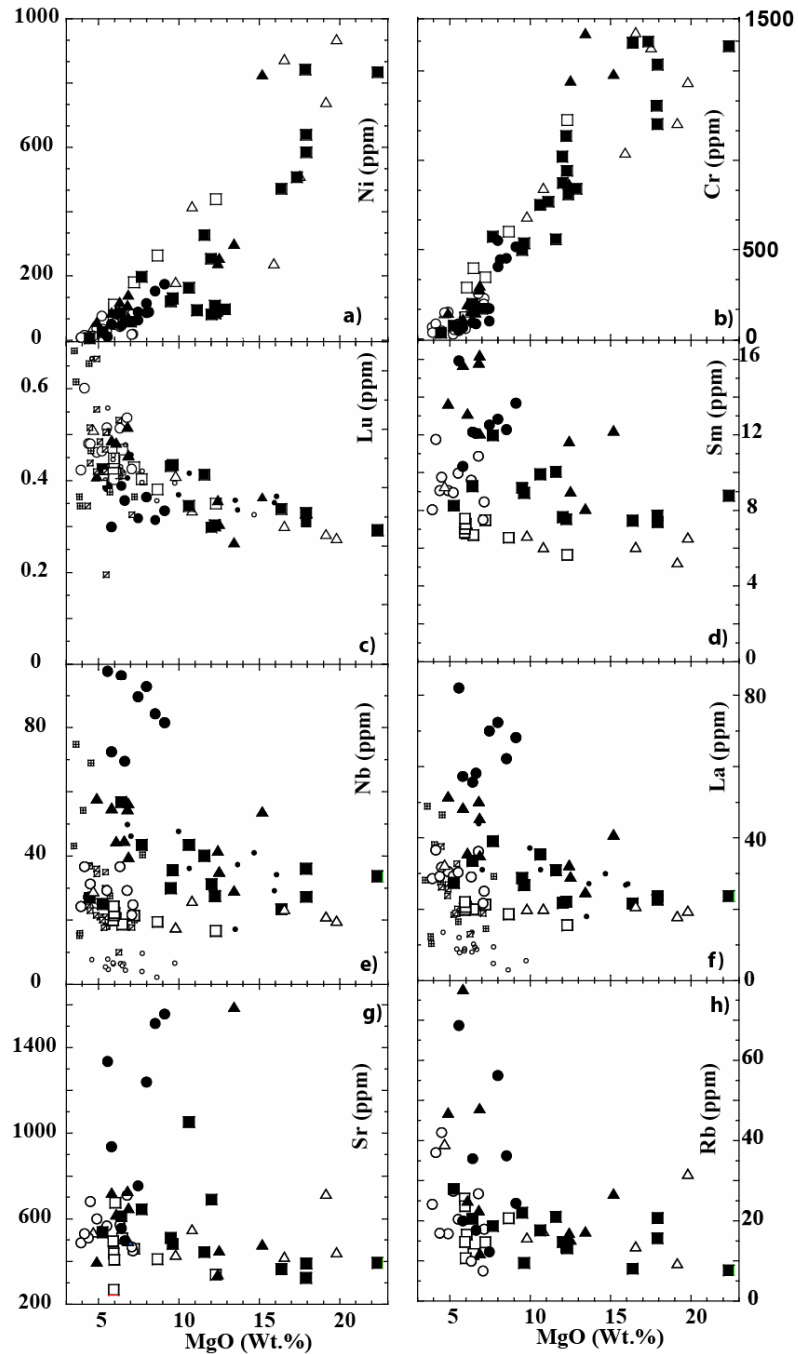


Figure 6. MgO vs. selected trace elements for Maychew lavas. The HT1 (small crossed rectangle), HT2 (shaded dots) and LT (small open circle) basalts are shown for comparison on c, e & f. HT2 overlaps fields of sequence 2 & 3, HT1 overlaps fields of evolved sequence 3, Sequence 4, 5 and 6, whereas LT basalts do not overlap any of Maychew sequences (when incompatible elements such as Nb & La are considered).

The sequence 1 and 2 show the greatest relative enrichment in P_2O_5 , FeO_{total} and TiO_2 . In contrast, the upper sequences 3, 4, 5, and 6 shows relatively low P_2O_5 , FeO_{total} , and TiO_2 , but highly enriched in SiO_2 and Al_2O_3 . Between 1 & 2, sequence 1 shows lower SiO_2 (45-42 Wt. %), Al_2O_3 (12-8.5 Wt.%) and TiO_2 (5.4-3.6 Wt.%) and higher CaO (15-12 Wt.%) and FeO_{total} (18.2-16 Wt.%) (Figs. 4 & 5). Compared to 4, sequence 3 shows higher P_2O_5 , K_2O and TiO_2 and lower Al_2O_3 and CaO than, however, their SiO_2 , Na_2O (not shown) and FeO_{total} concentrations appear equally variable and scattered in both sequences. Moreover, CaO concentrations in sequence 4 lavas are higher than that of sequences 3 and 2 lavas with respect to MgO content. In the case of Na_2O and K_2O , they are scattered considerably in all the sequences and suggest secondary redistribution of Na and K. However, the extent of secondary alteration has also been evaluated using K_2O/P_2O_5 , which is > 1 (not shown) in all types except for the three basanite samples from sequence 1, indicating minimum influence of subaerial weathering. K_2O/P_2O_5 ratio is used in evaluating the effect of subaerial weathering in mafic lavas, where K is easily leached by secondary alteration and P is not.

4.3. Trace element compositions of mafic rocks from the Maychew flood basalt section

The compatible elements Ni and Cr (Fig. 6a & b) show perfect linear relationship with MgO and suggest the control of olivine, clinopyroxene, and Cr-spinel. Presence of olivine, clinopyroxene or/and Cr-spinel well explains high contents of MgO , Ni, and Cr in picrite and ankaramite (Seq. 5, 3 & 2). They are possibly mantle-derived melts having $\sim 11\%$ MgO (Skovgaard et al., 2001). Crystal fractionation is the preferred mechanism for Cr depletion as its abundance is not expected to vary under conditions of increasing partial melting (Pearce and Norry, 1979). The incompatible elements La, Nb, Lu, Sm, Sr and Rb (Figs. 6c, d, e, h & f) with some scatter increase with decreasing MgO . The basanites (Seq.1) at the base of Maychew flood basalt section has the highest relative enrichments of incompatible trace elements (La & Nb). The sequence 2, alkaline basalts and ankaramites, has intermediate contents and in the upper sequence 3, 4, 5 and 6 the trace elements sequentially depleted upwards with some scatter. Basanites display relatively fractionated rare earth element (REE) patterns ($(La/Lu)_N = 30-18$ (subscript N denotes chondrite normalization) compared to other sequences (Seq.2, $La/Lu_N = 16-9$; Seq. 3, $La/Lu_N = 14-7$; Seq. 4, $La/Lu_N = 9-6$; Seq. 5, $La/Lu_N = 10-6$; Seq. 6, $La/Lu_N = 7-5$) (Fig. 7d). So, there exist a good correlation of rock types with varying geochemical enrichments

such as an increase in $(La/Lu)_N$ with TiO_2 and a general decrease in Al_2O_3 and SiO_2 towards the base (Figs. 6 & 7).

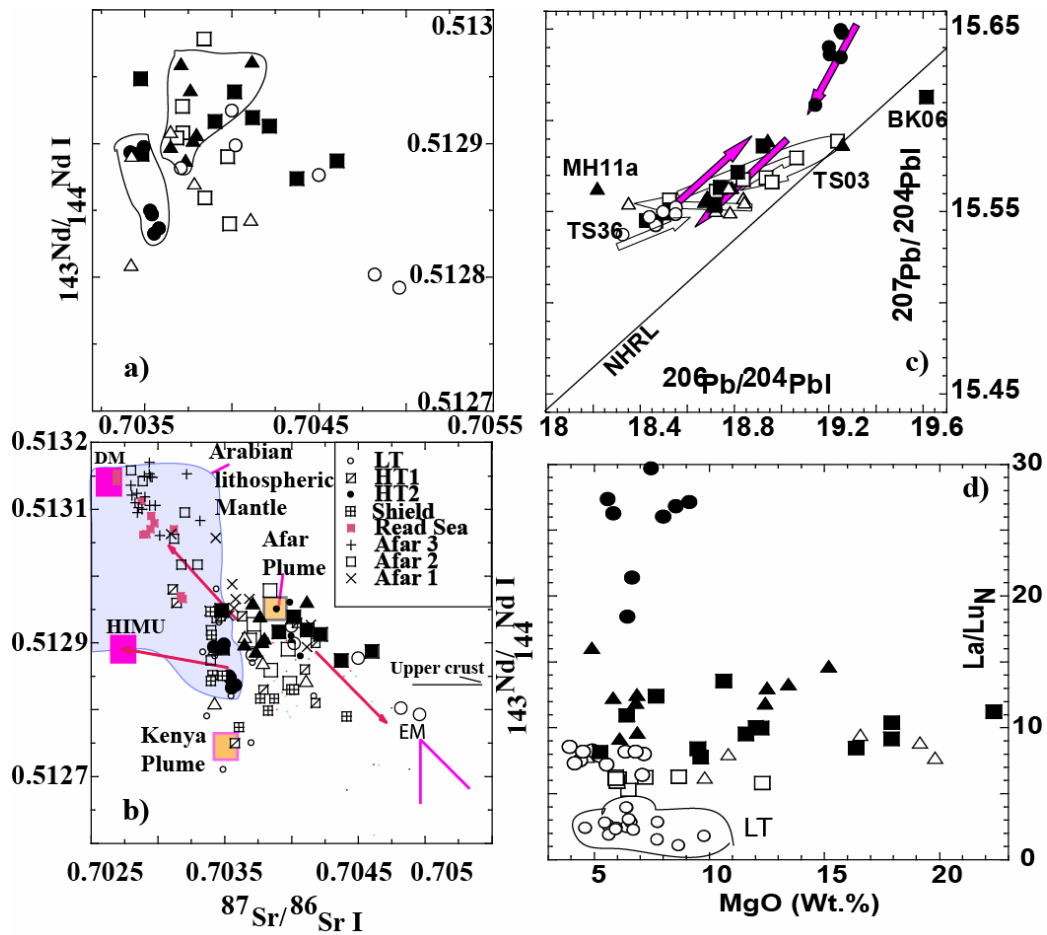


Figure 7. a). $^{87}Sr/^{86}Sr$ - $^{143}Nd/^{144}Nd$ initial ratio plot, b). $^{87}Sr/^{86}Sr$ - $^{143}Nd/^{144}Nd$ initial ratio plots comparing Maychew lavas with volcanics in the region, c). $^{207}Pb/^{204}Pb$ - $^{206}Pb/^{204}Pb$, plot d) MgO Vs La/Lu_N plots for Ethiopian flood basalt section at Maychew [The data range for LT, HT1, & HT2 is from Pik et al. (1999). Afar group data range is from Schilling et al. (1992). The Red Sea data is from Vidal et al. (1991). Arrows in c mimics way up. Note: in b, DM- Depleted mantle; HIMU- high- μ ; EM- Enriched mantle; in c, NHRL Northern-Hemisphere Reference-Line; BK-06, TS03; and MH11a are samples which plots differently from the sequence.

4.4. Isotope variations

Among the analyzed isotopes, Sr-Nd isotope data (Fig. 7 a & b) when plotted, two clusters are formed, one with restricted and low Sr (0.70356-0.70345) and Nd (0.51290-0.51284) isotopic compositions, defined by sequence 1 samples, and the other cluster with relatively higher Sr

(0.7052-0.7036) and Nd (0.51296-0.5127), defined by sequence 2. Other sequences show more scattered patterns.

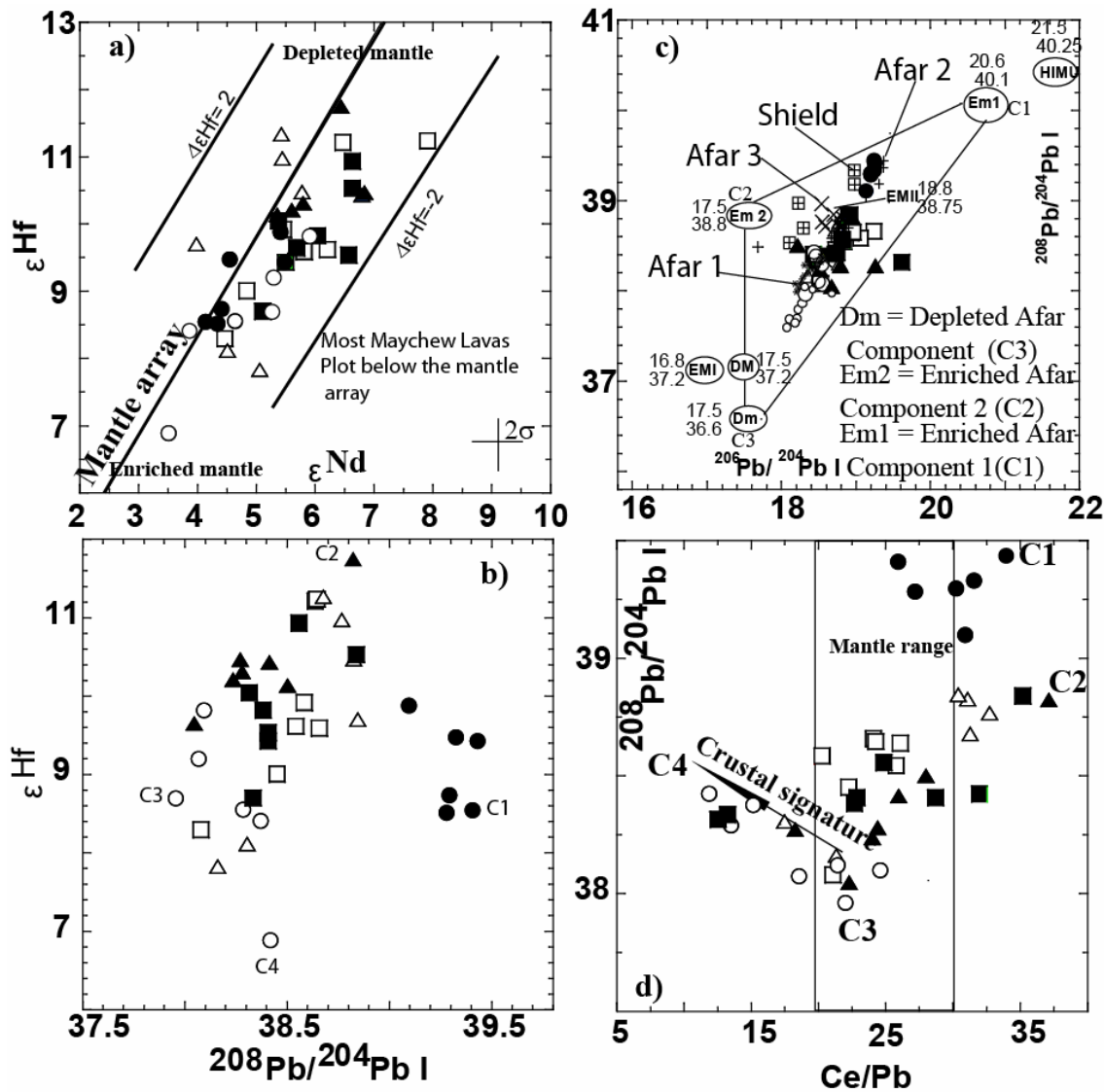


Figure 8. a). $\epsilon_{\text{Hf}}-\epsilon_{\text{Nd}}$, b). ϵ_{Hf} Vs $^{208}\text{Pb}/^{204}\text{Pb}$ initial, c). $^{208}\text{Pb}/^{204}\text{Pb}$ Vs $^{206}\text{Pb}/^{204}\text{Pb}$, and d). $^{208}\text{Pb}/^{204}\text{Pb}$ Vs Ce/Pb plots for Maychew flood basalt samples. C1, C2, C3, and C4 in b, indicate mixing components defined by the Maychew lava sequence. The three Afar plume mantle end components further elucidated in Figure 8c where sequence 1 and 0 Ma Afar group 2 (Schilling et al., 1992) displaced towards the highest $^{206}\text{Pb}/^{204}\text{Pb}$ ratios. In Figure 8d most samples are plotted within and above the proposed mantle range, however, some samples are (lower part of sequence 3 and upper part of sequence 4 & 5) are displaced towards C4, crustal component. Symbols for Maychew lavas are as in Figures 4 & 7.

Pb isotopic compositions (Figs. 7c & 8) also show a systematic variation from base to top, with sequence 1 having the most radiogenic signature ($^{206}\text{Pb}/^{204}\text{Pb} = 19.10\text{-}19.30$, $^{207}\text{Pb}/^{204}\text{Pb} = 15.60\text{-}15.65$) while sequence 4 indicating lower values ($^{206}\text{Pb}/^{204}\text{Pb} = 18.20\text{-}18.56$, $^{207}\text{Pb}/^{204}\text{Pb} = 15.51\text{-}15.55$). Sequences 2 and 3 lavas display similar $^{206}\text{Pb}/^{204}\text{Pb}$ and $^{207}\text{Pb}/^{204}\text{Pb}$ ratios. Sequence 6 samples on the other hand though show lower $^{207}\text{Pb}/^{204}\text{Pb}$ (Fig. 7c) values, they are higher $^{206}\text{Pb}/^{204}\text{Pb}$ than in the samples from sequences 2, 3, 4 and 5. Similarly lavas of sequence 1 and 4 are relatively less radiogenic $^{176}\text{Hf}/^{177}\text{Hf}$ than sequence 2 (Fig. 8a). In other sequences the data show slight scattered pattern (Fig. 7c). These variations are quite different from what has previously been reported for northwestern Ethiopian flood basalt province (Pik et al., 1999).

5. CONCLUSION

- The HT1+HT2 zone of northwestern Ethiopian flood basalt province show sequential compositional variations (Seq 1-Seq 6). The sequence 2 & 3 are similar to HT2 of Pik et al (1998), whereas Sequence 4 overlaps the ranges of HT1 basalts of Pik et al (1998). Sequence 1, basanites is described for first time in this study and enriched in incompatible elements more than the HT2 basalts. Sequence 5 and 6 show different chemical variations in isotopic ratios than HT1 and HT2.
- Smooth increase of $(\text{La}/\text{Lu})_N$ ratios down the sequence reflect the general decrease of degree of partial melting of heterogeneous packages of mantle materials.
- The systematic geochemical variations in lavas are interpreted to reflect mixing of three mantle components, with minimal crustal in-put as a fourth component.
- The enriched sequence 1 has very similar geochemistry to HIMU-type ocean island basalts, and this ascribed as end member to the most enriched Afar plume component 1 involved in the initial continental break-up.
- The second enriched component is defined on the basis of the geochemistry of the samples from sequences 2 & 3 which reflect the second enriched component in Ethiopian flood basalt, previously described (Pik et al., 1999) as high-Ti2 basalts assumed to be the Afar Plume component.
- The third component would be the depleted one as defined by samples from sequence 4,

which partly overlaps the range previously reported for low-Ti basalts (Fig. 8; Pik et al., 1999).

- The difference between the 1st and 2nd enriched Afar Plume components might be due to variable lithospheric signatures, with the 2nd enriched Afar plume component having more lithospheric material.
- The fourth component is crustal signature (Fig. 8d) which invariably affected all the lava sequences. Crustal signatures are quite prominent in sequences 3 & 4 compared to others.

6. ACKNOWLEDGEMENTS

Kurkura Kabeto acknowledges financial support from Japanese Society for Promotion of Science (JSPS) and also by the program for the ‘Center of Excellence for the 21st Century in Japan’ to ISEI, Okayama University. I thank Prof. Talat Ahmad and Dr. K. Bheemalingeswara, and the editor Dr. Tadesse for their constructive comments on the manuscript.

7. REFERENCES

- Ayalew D., Barrey, P., Marty, B., Reisberg, L., Yirgu, G & Pik. R. 2002. Source, genesis, and timing of giant ignimbrite deposits associated with Ethiopian continental flood basalts. *Geochemica et Cosmochimica Acta*, **66**: 1429-1448.
- Berhe, S.M., Desta, B., Nicoletti, M & Tefera, M. 1987. Geology, geochronology and geodynamic implications of the Cenozoic magmatic province in W and SE Ethiopia. *J. Geol. Soc. London*, **144**: 213-226.
- Coulie, E., Quidelleur, X., Gillot, P.Y., Courtillot, V., Lefevre, J.C & Chiesa, S. 2003. Comparative K–Ar and Ar/Ar dating of Ethiopian and Yemenite Oligocene volcanism: implications for timing and duration of the Ethiopian traps. *Earth and Planetary Science Letters*, **206**: 477–492.
- Hofmann, C., Courtillot, V., Feraud, G., Rochette, P., Yirgu, G., Ketefo, E & Pik, R. 1997. Timing of the Ethiopian flood basalt event and implications for plume birth and global Change. *Nature*, **389**: 838-841.
- Jones, P. 1976. Age of the lower flood basalts of the Ethiopian plateau. *Nature*, **261**: 567–569.

- Kabeto, K., Tanaka, R., Makishima, A & Nakamura, E. 2006. Geological and geochemical evidence for sequential compositional variations in Mid-Tertiary Ethiopian Flood Basalt Province: implications for the Afar Plume enriched component. 2nd AASP Int. Symp. Cameroon Volcanic Line, East African Rift System, the underlying Mantle and Evolution of the African Continental Crust. Dar es Salaam, Tanzania, Extended Abstract, 1: 19-25.
- Kabeto, K., Sawada, Y., Bussert, R & Kuester, D. 2004. Geology and Geochemistry of Maychew Volcanics, northwestern Ethiopian Plateau. International Conference on East African Rift system, Addis Ababa, Ethiopia. Extended Abstract 1 : 110-114.
- Kieffer, B., Arndt, N., Lapiere, H., Basitien, F., Bosch, D., Pecher, A., Yirgu, G., Ayalew, D., Weis, D., Gerram, D.A., Keller, F & Meugniot, C. 2004. Flood and Shield Basalts from Ethiopia: Magmas from the African Superswell. *J. Petrology*, **45**: 793-834.
- Kuritani, T & Nakamura, E. 2002. Precise isotope analysis of nanogram-level Pb for natural rock samples without use of double spikes. *Chemical Geology*, **186**: 31–43
- Kuritani, T & Nakamura, E. 2003. Highly precise and accurate isotopic analysis of small amounts of Pb using $^{205}\text{Pb}/^{204}\text{Pb}$ and $^{207}\text{Pb}/^{204}\text{Pb}$, two double spikes. *Journal of Analytical and Atomic Spectrometry*, **18**: 1464-1470.
- Kuster, D., Dwivedi, S. B., Kabeto, K., Mehary, K & Matheis, G. 2005. Petrogenetic reconnaissance investigation of mafic sills associated with flood basalts, Mekelle basin, northern Ethiopia: implication for Ni-Cu exploration. *J. Geochemical Exploration*, **85**: 63 – 79.
- Le Bas, M.J. 2000. IUGS reclassification of the high-Mg and picritic volcanic rocks. *J. Petrology*, **41**: 1467-1470.
- Lu, Y., Makishima, A & Nakamura, E. 2007. Purification of Hf in silicate materials using extraction chromatographic resin, and its application to precise determination of $^{176}\text{Hf}/^{177}\text{Hf}$ by MC-ICPMS with ^{179}Hf spike. *J. Analytical and Atomic Spectrometry*, **22**: 69-76, doi:10.1039/b610197f.
- Makishima, A & Masuda, A. 1993. Primordial Ce isotopic composition of the solar system. *Chem. Geology*, **106**: 197-205.
- Makishima, A & Nakamura, E. 1991. Determination of major, minor and trace elements in silicate samples by ICP-QMS and ICP-SFMS applying isotope dilution-internal

- standardization (ID-IS) and multi-stage internal standardisation. *Geostandards and Geoanalytical Research*, **30**: 245-271.
- Makishima, A & Nakamura, E. 1997. Suppression of matrix effects in ICP-MS by high power operation of ICP: Application to precise determination of Rb, Sr, Y, Cs, Ba, REE, Pb, Th and U at ng g⁻¹ levels in milligram silicate samples. *Geostandards Newsletter*, **21**: 307-319.
- Makishima, A., Nakamura, E & Nakano, T. 1997. Determination of boron in silicate samples by direct aspiration of sample HF solutions into ICP-MS. *Analytical Chemistry*, **69**: 3754–3759.
- Makishima, A., Nakamura, E & Nakano, T. 1999. Determination of zirconium, niobium, hafnium and tantalum at ng g⁻¹ levels in geological materials by direct nebulization of sample HF solution into FI-ICP-MS. *Geostandards Newsletter*, **23**: 7–20.
- Merla, G. 1979. Explanation to the Geology map of Ethiopia and Somalia 1:2,000,000 Scale. Department of Geology and Paleon., University of Florence, Italy
- Moriguti, T., Makishima, A & Nakamura, E. 2004. Determination of lithium contents in silicates by isotope dilution ICP-MS and its evaluation by isotope dilution thermal ionization mass spectrometry. *Geostandards and Geoanalytical Research*, **28**: 371-382
- Nakamura, E., Makishima, A., Moriguti, T., Kobayashi, K., Sakaguchi, C., Yokoyama, T., Tanaka, R., Kuritani, T & Takei, H. 2003. Comprehensive geochemical analysis of small amounts (<100 mg) of extraterrestrial samples for the analytical competition related to the sample-return mission, MUSES-C. Institute of Space and Astronautical Science Report, SP16: 49-101.
- Pearce, J. A & Norry, M. J. 1979. Petrogenetic implications of Ti, Zr, Y, and Nb variations in volcanic rocks. *Contributions to Mineralogy and Petrology*, **69**: 33–47.
- Pik, R., Daniel, C., Coulon, C., Yirgu, G., Hofman, C & Ayalew, D. 1998. The northwestern Ethiopian flood basalts: Classification and spatial distribution of magma types. *J. Volcanol. Geotherm. Res.*, **81**: 91-111.
- Pik, R., Daniel, C., Coulon, C., Yirgu, G & Marty, B. 1999. Isotopic and trace element signatures of Ethiopian flood basalts: Evidence for plume lithosphere interactions. *Geochim. Cosmochim Acta*, **63**: 2263-2279.

- Piccirillo, E.M., Justin-Visentin, E., Zanettin, B., Jottron, J. K & Treuil, M. 1979. Geodynamic evolution from plateau to rift: major and trace element geochemistry of the central eastern Ethiopian plateau volcanics. *Neues Jahrbuch fur geologie un Palantologie*, **258**: 139-79.
- Rochette, E, Tamrat, E., F6raud, G., Pik, R., Courtillot, V., Ketefo, E. 1998. Magnetostratigraphy and timing of the Oligocene Ethiopian traps. *Earth and Planetary Science Letters*, **164**: 497-510.
- Schilling, J.-G., Kingsley, R. H, Hanan, B.B & McCully B.L. 1992. Nd-Sr-Pb isotopic variations along Gulf of Aden Evidence for Afar Plume & lithosphere interaction. *J. Geophys Res.*, **97**: 10927-10966.
- Skovgaard, A.C., Storey, M., Baker, J., Blusztajn, J & Varet, J. 2001. Geochemistry of basalts from Manda Hararo, Ethiopia: LREE-depleted basalts in Central Afar. *Lithos*, **69**, 1-13.
- Tanaka, R., Makishima, A & Nakamura, E. 2007. Hawaiian double volcanic chain triggered by an episodic involvement of recycled material: Constraints from temporal Sr–Nd–Hf–Pb isotopic trend of the Loa-type volcanoes. *Earth and Planetary Science Letters*, **30**: 450-465.
- Takei, H. 2002. Development of precise analytical techniques for major and trace element concentrations in rock samples and their applications to the Hishikari Gold Mine, southern Kyushu, Japan. PhD thesis, Okayama University, 164p.
- Vidal, P., Deniel, C., Vellutini, P. J., Piguët, P., Coulon, C., Vincent, J & Audin, J. 1991. Changes of mantle source in the course of a rift evolution. *Geophysical Research Letters*, **18**: 1913-1916.
- Yoshikawa, M & Nakamura, E. 1993. Precise isotope determination of trace amounts of Sr in magnesium-rich samples. *J. Mineralogist, Petrologist & Economic Geologist*, **88**: 548-561.
- Yokoyama T., Makishima A & Nakamura E. 1999. Evaluation of the coprecipitation of incompatible trace elements with fluoride during silicate rock dissolution by acid digestion. *Chemical Geology*, **157**: 175-187.